Diamond & Related Materials 24 (2012) 210–214

Contents lists available at SciVerse ScienceDirect

Diamond & Related Materials

journal homepage: www.elsevier.com/locate/diamond

Microwave plasma reactor design for high pressure and high power density diamond synthesis ☆

Yajun Gu [a], J. Lu [a], T. Grotjohn [a,b], T. Schuelke [a,b], J. Asmussen [a,b,*]

[a] Michigan State University, East Lansing, MI 48824, USA
[b] Fraunhofer USA, Center for Coatings and Laser Applications, East Lansing, MI 48824, USA

ARTICLE INFO

Available online 31 January 2012

Keywords:
Microwave plasma assisted CVD
Diamond synthesis
High pressure
High power density
Single crystalline diamond
Microwave plasma reactor design

ABSTRACT

The design and performance of an improved microwave plasma assisted chemical vapor deposition (MPACVD) reactor is described. This reactor operates with high power densities and at pressures up to 300 torr. Differences from earlier MPACVD reactor designs [4] include an increase in applicator and dome size and the excitation of the applicator with a new "hybrid "TM_0/TEM_{001}" mode. The reactor is experimentally evaluated by synthesizing single crystal diamond (SCD) at pressures from 180 to 300 torr with absorbed power densities between 400 and 1000 W/cm^3. Without N_2 addition SCD growth rates as high as 75 μm/h were observed. A SCD growth window between 950 °C and 1300 °C was identified and within this growth window growth rates were 1.2 to 2.5 times greater than the corresponding growth rates for earlier reactor designs. SCD characterization by micro-Raman spectroscopy, SIMS, and by IR-UV transmission spectroscopy indicated that the synthesized SCD quality is that of type IIa diamond.

1. Introduction

It is now understood that microwave plasma assisted chemical vapor deposition (MPACVD) diamond growth rates and quality can be improved by creating high power density microwave discharges operating at pressures above 160 torr [1–3]. Thus this study investigates the experimental performance of MPACVD reactors that are specifically designed to operate at pressures above 180 torr. These reactors take advantage of the enhanced deposition chemistries and physics that exist at higher pressures and are robust and optimized for operation with high absorbed microwave power densities within the 180–300 torr pressure regime. Here we describe a new reactor design that, in comparison with earlier designs, has both a larger diameter cavity applicator and a larger discharge chamber. The cavity is excited with a new/different hybrid electromagnetic mode. The performance of this new reactor is briefly summarized below and the results of exploratory single crystal diamond (SCD) synthesis experiments are also compared with the experimental performance of earlier MPACVD reactor designs [4,5].

2. Background

The formation of microwave discharges at high pressures was first observed and investigated many years ago [6–8]. High pressure microwave discharges have been applied as plasma sources for electrothermal thruster space engines [9–11] and as high pressure, microwave discharge light sources [12]. A visual example of how the microwave discharge behaves as pressure increases is displayed in Fig. 2 of Ref. [4]. As shown, as the pressure increases the discharge shrinks, constricts and becomes more intense.

At pressures of 100 torr or more, microwave discharges in hydrogen and methane gas mixtures separate from the reactor walls. They become freely floating and assume shapes that are related to the shape of the impressed electromagnetic (EM) fields. At very high pressures microwave discharges become very non-uniform, intense and "arc like". They may even move about the discharge chamber as they react both to buoyant and convective forces caused by the gas flows around and within the discharge. Plasma densities for 2.45 GHz hydrogen discharges operating at pressures from 100 to 200 torr are estimated to be about 10^{12} cm^{-3} [13]. At pressures greater than 150 torr, microwave discharges in hydrogen and methane gas mixtures have neutral gas temperatures in excess of 3000 K. These discharges have high densities of radical species, i.e. H and CH_3 radicals, which enable increased diamond growth rates at high pressures [2].

Since high pressure microwave plasma discharges behave very differently from the typical lower pressure discharges they require methods of discharge control and microwave applicator and plasma reactor design that take into account their distinctly unique nature. As pressure increases the size, the spatial location and the shape of the very hot, non-uniform plasma must be controlled so that optimal CVD diamond synthesis is achieved. Thus in our designs we provide substrate position adjustments that enable the substrate to be

☆ Presented at NDNC 2011, the 5th International Conference on New Diamond and Nano Carbons, Suzhou, China.

* Corresponding author at: Michigan State University, East Lansing, MI 48824, USA.
E-mail address: asmussen@egr.msu.edu (J. Asmussen).

0925-9635/$ – see front matter © 2012 Elsevier B.V. All rights reserved.
doi:10.1016/j.diamond.2012.01.026

positioned up into and in good contact with the discharge as pressure is varied. This enables the optimal, independent positioning of the substrate with respect to the discharge as pressure varies, and yields high deposition rates. Thus at high pressures the independent positioning of the discharge with respect to the substrate position becomes an additional experimental variable.

There are a number of other important issues associated with utilizing high pressure MPACVD discharges for diamond synthesis. First, because of the discharge's high gas temperatures, the substrate must be appropriately cooled to the desired deposition temperature. The reactor walls, in contrast to the substrate, must be protected from the intense high temperatures of the discharge and from the active discharge species. As a result it is desirable that the hot discharge be separated and placed out of direct contact from the reactor walls. In our new reactor design both the metal and dome walls are removed from the discharge zone. This reduces plasma and radical species wall interactions and also reduces the conductive and convective discharge heat flux losses to the walls.

3. Reactor design

Here a new reactor design, Reactor C, is presented and compared with two earlier reactor designs, Reactors A and B. Reactor A, which was designed to operate within the 20–160 torr regime, has been described earlier [5,14] and is used in this investigation as the reference reactor. Recently a second reactor, Reactor B, was also designed to produce stable, high absorbed power density discharges within the 180–240 torr pressure regime. The details of Reactor B's design, i.e. the dimensions such as R_1, R_2, L_1, etc., and its performance synthesizing polycrystalline diamond were recently presented [4]. A cross section of Reactor B is displayed in Fig. 1 (a). Major differences between Reactor A and B are: (1) the substrate holder area of Reactor B is reduced by factor of four, (2) the substrate holder position, $Z_S = L_1 - L_2$, is variable from +1 mm to −10 mm around the $Z = 0$ plane, and (3) the cylindrical applicator is excited in the "hybrid TM_{013}/TEM_{001}" mode.

The basic design features of Reactor C are: (1) single mode excitation, (2) internal applicator matching, (3) adjustable substrate position, Z_S, (4) variable electromagnetic focus at the substrate position and (5) the excitation of a "non-classical" electromagnetic (EM) applicator mode. The tunability and the experimental versatility of the design allows not only excellent discharge matching but also the control of the position, size, shape and intensity of the microwave discharge. An additional advantage of the new reactor design is its ability by varying L_s to experimentally determine new, useful, and "non-classical", applicator EM excitation modes that enable diamond synthesis. Hence, during the Reactor C design process we were readily able to experimentally search for and identify a new and very useful hybrid excitation electromagnetic mode.

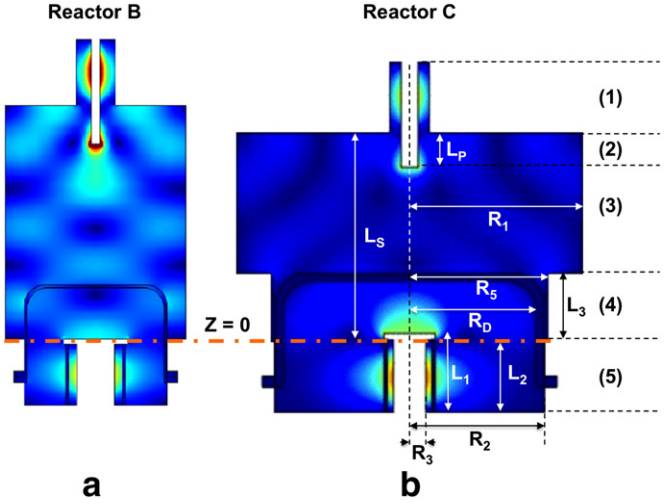

Fig. 1. Cross sections of Reactors B and C. The electromagnetic field excitation of Reactor B is the "hybrid TM_{013}/TEM_{001}" mode and of Reactor C is the "hybrid TM_0/TEM_{001}" mode. The electric field patterns displayed are calculated for resonant applicator excitation without a discharge.

As displayed in Fig. 1 (b) Reactor C is composed of the five cylindrical sections including the coaxial input section (1) and additional sections (2) through (5). The major differences between Reactor B and Reactor C designs are that in Reactor C: (1) the applicator and dome diameters, i.e. 2 R_1 and 2 R_D, have been increased respectively from 17.78 cm to 30.48 cm and from 13.02 cm to 21.6 cm and the dome height, h, was increased from 9.47 cm to 10.86 cm, (2) the applicator has an additional cylindrical section, i.e. section (4), providing an abrupt step change in applicator radius from section (3) and (3) the applicator is excited in the "approximate" TM_0/TEM_{001} hybrid mode. In sections (2)–(4) the mode is TM and phi symmetric, hence the notation TM_0. Because each section has a length that is short with respect to the guided wave length, the EM field patterns in these sections are not easily related to the empty classical cylindrical cavity modes. Thus the notation TM_0 is adopted here as the identification for the EM mode in sections (2)–(4). Due to this hybrid mode excitation, the height, L_s, above the $Z = 0$ plane was reduced from ~21 cm in Reactor B to ~16 cm in Reactor C. However the substrate holder/cooling stage area in section (5) has the same dimensions as the holder/cooling stage in Reactor B.

As shown in Fig. 1 Reactor C has larger radii, i.e. R_1, R_2, R_D, etc., than Reactor B. The increased reactor and dome sizes remove the reactor walls further from the discharge zone and thus reduce wall heating and plasma/radical species wall interactions. The variation of reactor radii versus the five cylindrical sections has an additional benefit. Microwave energy is coupled and impedance matched into the reactor, by varying L_S and L_P. The EM energy that is transmitted to the discharge zone above the substrate holder is first defocused in sections (1)–(3) and then, by reducing the radius R_5 and by varying L_1 and L_2, is refocused onto the substrate holder in sections (4)–(5).

The first prototype realization of this design has the following dimensions; L_P~3 cm; L_S~16.2 cm; $R_1 = 15.24$ cm; $R_2 = 10.16$ cm; $R_3 = 1.84$ cm; $h = 10.86$ cm; $R_5 = 12.07$ cm; L_1 and L_2~6.12 cm; -0.8 cm$< Z_S <$0.5 cm; and $L_3 = 7.32$ cm. Reactor C has four mechanically independent cavity applicator adjustments: (1) variable coupling probe length L_P, (2) variable substrate holder length L_1, (3) variable top plate sliding short L_S, and (4) variable conducting short plate L_2. These enable process optimization and impedance matching and are varied for discharge control as input power, pressure, gas flow, substrate holder design, etc. are varied. Fig. 2 displays an example of how the electric field varies above the substrate holder as Z_S is varied from +4 mm to −6 mm. As shown the electric field increases and is focused as Z_S is adjusted from above to below the $Z = 0$ plane.

4. Experimental procedures

SCD was grown on commercially available 3.5 mm by 3.5 mm synthetic, high pressure high temperature (HPHT) SCD substrates. Each experimental run was limited to less than 24 hours. Before each experimental run the HPHT substrate was chemically cleaned and then was subjected to a 1–4 h H_2 (5.5 N) plasma etching pretreatment before introducing 2–9% methane (5 N) into the feed gas. Substrate temperatures (T_S) as reported later in Figs. 5 and 6 were measured by using an infrared pyrometer with one fixed wavelength (one-color) at 0.96 μm. Two-color pyrometer temperature measurements were also taken. Under the same conditions the two color measurements were approximately 100 K higher than the one-color

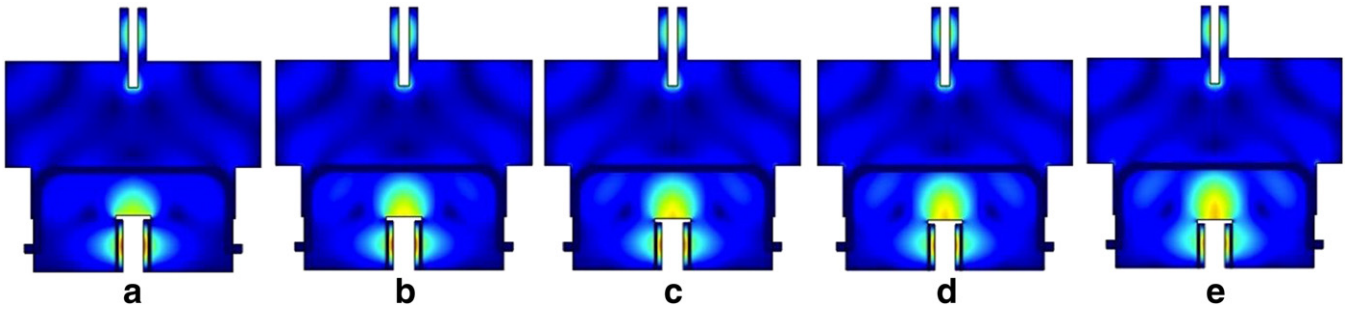

Fig. 2. Electric field strength variation in the cavity applicator with varying Z_S. $Z_S = +4$ mm, $+2$ mm, 0 mm, -4 mm, -6 mm for image (a) … (e).

measurements. Film thicknesses were measured by a linear encoder. The growth thickness for each experimental run was determined as the average of five measurement points on the top surface of the diamond. One measurement point was in the center of the grown diamond and the other four points were measured near each of the corners.

The discharge was ignited at low pressures of a few torr using a low input power level of 1.25 kW and then once ignited the input power was gradually increased as the pressure was increased to the appropriate higher pressure deposition conditions. Once the mode ignition tuning positions, i.e. L_S, L_P and Z_S, were determined the discharge always ignited only on the top of the substrate holder and no additional tuning was necessary as the reactor was adjusted for CVD process conditions.

Experiments were performed without any N_2 addition. The total gas flow rate was kept constant at approximately 400 sccm. The growth rate is strongly dependent on N_2 impurity levels [15]. We have estimated that the impurities of N_2 in the feed gases and from any leaks in the vacuum system. i.e. our "no N_2 addition condition", yields an equivalent N_2 input of ~5 ppm of the input gas flow.

All substrate holders used in the experiments were holders of the type shown in Fig. 3. The differences between holders were the pocket dimensions and the thicknesses. The substrate deposition temperature, T_S, was varied by varying the dimensions A and B. All experimental runs reported here involved one continuous run using one pocket holder.

The SCD quality was evaluated by Raman spectroscopy, IR–UV transmission measurements and SIMS analysis. Raman spectroscopy was performed using a 514.5 nm Ar ion laser with a spot size of 20–30 μm and a resolution of 0.2 cm^{-1}. The Raman measurements on each grown sample were compared with a type IIIa diamond reference sample from Element Six. This low absorption, reference sample has a nitrogen impurity level of ~30 ppb and as measured by us a Raman FWHM of 1.64 cm^{-1}.

5. Experimental performance

5.1. Discharge absorbed power density

The discharge absorbed power densities for Reactors A, B and C were measured over the experimental 60–300 torr regime and the results are displayed in Fig. 4. The plasma volume was determined experimentally from size calibrated photographs of the discharge versus pressure. For each data point in Fig. 4 the discharge volume was defined as the white central core of the discharge (see Fig. 2 of Ref. [4]), i.e. as the volume of the brightest luminescence of the discharge. Then the discharge power density at each pressure was calculated as the absorbed microwave power divided by the plasma volume.

As expected the discharge power density for all three reactors increases as pressure increases. In the lower pressure regime of 60–180 torr Reactors B and C have similar discharge power densities versus pressure and their power densities are larger by a factor of 4–5 over the discharge power densities of Reactor A. For example, at a constant pressure of 140 torr the power density for Reactor A is 45 W/cm^3 while the power density for Reactor B is 210 W/cm^3. Reactors B and C have the same substrate holder area, which is smaller than in Reactor A. Thus one important conclusion from observing the data in Fig. 4 is that at a given pressure the discharge power density increases inversely proportional to the substrate holder area. As indicated earlier [4] the fourfold reduction in substrate holder area increases the discharge power density by a factor of about 4–5.

When the pressure is increased above 180 torr, power densities as high as 300–1000 W/cm^3 are achieved. As pressure increases beyond 200 torr the power densities for Reactor C become increasingly greater than those of Reactor B. While we do not know the exact reason for this difference we speculate that at the higher pressures reactor geometry differences between the two reactors produce different internal gas flows within and around the discharge resulting in different absorbed discharge power densities.

5.2. Growth rate versus pressure

A series of exploratory experiments of SCD growth rate versus pressure, methane concentration, and substrate temperature were performed in Reactors A, B and C and the results are displayed in Fig. 5. Clearly the maximization of the growth rate at each data point is a multivariable optimization problem. At each of the data points shown in Fig. 5 the total flow rate was held at ~400 sccm and the substrate position, Z_S, for each reactor was held constant at an optimized (high growth rate) position. The optimized Z_S positions are -3.6 mm for Reactor B and -4.8 mm for Reactor C. The input powers ranged from 3 kW for Reactor A, between 2.1–2.3 kW for Reactor B and 1.9–2.1 kW for Reactor C. The exploratory experimental data in Fig. 5 show that there are important increases in SCD growth rates for Reactors B and C over Reactor A at lower pressures. A comparison of Figs. 4 and 5 suggests that the increased growth rates in Reactor C are related in part to the increased discharge power density due to both the smaller substrate holder and operation at higher pressures.

A more precise comparison between reactors B and C is made in Fig. 6 where the performance of the reactors is compared under

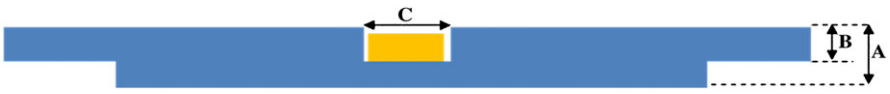

Fig. 3. Side cross sectional view of generic pocket holder.

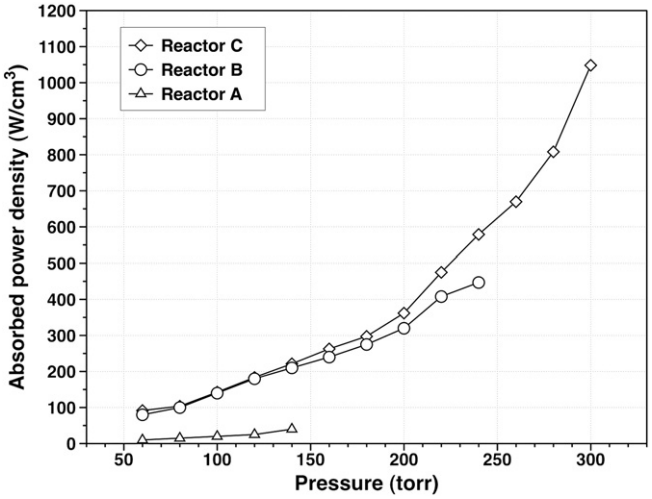

Fig. 4. Absorbed power densities versus pressure for Reactors A, B and C.

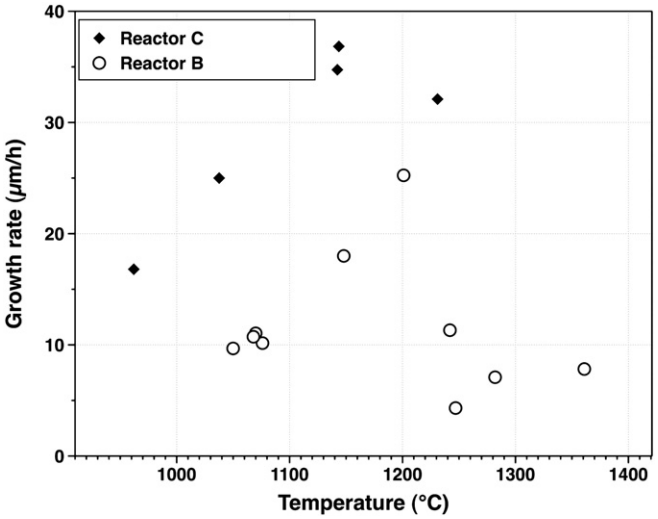

Fig. 6. SCD growth rate versus temperature for Reactors B and C.

similar experimental conditions. For each experimental data point there are at least eight important experimental variables: (1) pressure, (2) substrate temperature, (3) substrate position, Z_S, (4) substrate holder thickness (see Fig. 3), (5) methane concentration, (6) flow rate, (7) absorbed power density, and (8) reactor design/geometry. In the comparison between Reactors B and C shown in Fig. 6 both reactors were operated under the same input variable conditions, i.e. 240 torr, fixed Z_S, the fixed generic substrate holder configuration shown in Fig. 3, $CH_4/H_2 = 5\%$, and a constant total flow rate of ~400 sccm. Under these input conditions a series of experiments versus substrate temperature were performed for both reactors B and C operating with the approximate absorbed power density conditions that are indicated in Fig. 4. Fig. 6 identifies a SCD growth window between 950 and 1300 °C, where the growth rate exhibits a maximum between 1125 and 1225 °C. Under these conditions the maximum growth rate for Reactor B is about 25 μm/h at 1200 °C and 38 μm/h at 1150 °C for Reactor C. Within this growth window the growth rates for Reactor C are 1.2–2.5 times greater than the corresponding growth rates for Reactor B. This suggests that the higher power densities of Reactor C (see Fig. 4) result in higher deposition rates; i.e. changes in reactor design/configuration result in higher power densities and also higher deposition rates.

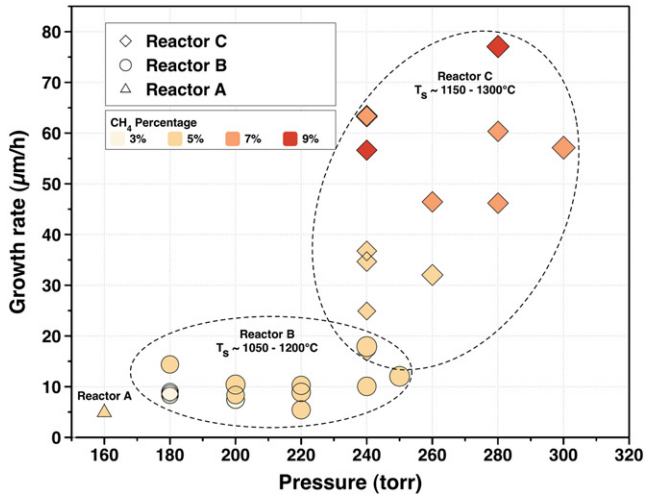

Fig. 5. SCD synthesis—growth rate versus pressure for Reactors A, B and C.

6. SCD diamond quality

Diamond plates were fabricated by removing the SCD CVD synthesized diamond from the seed by laser cutting and then the plates were mechanically polished. Examples of these plates are shown in Fig. 7.

The CVD synthesized SCD was characterized by micro-Raman spectroscopy, SIMS, and by IR–UV transmission spectroscopy. For Reactor C the Raman FWHM of the synthesized SCD ranged from 1.65 to 1.80 cm^{-1}. SIMS analysis shows 400–500 ppb N in the synthesized diamond (when N_2 was about 5 ppm in the gas phase). The IR

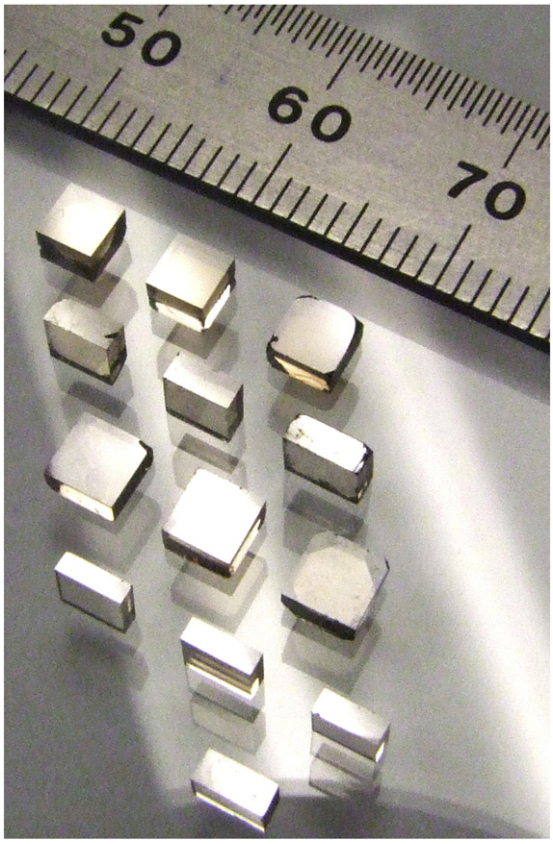

Fig. 7. Examples of CVD diamond plates.

transmission for all samples was similar to that associated with type IIa diamond, and the sub-bandgap ultraviolet optical absorption coefficients for the SCD synthesized with Reactor C were comparable to that reported for type IIa [16]; i.e. the absorption coefficient at 250 nm is between 4 and 7 cm^{-1}.

7. Summary

An improved microwave plasma assisted CVD reactor, Reactor C, has been designed and experimentally evaluated by growing single crystalline diamond over the 180–300 torr pressure regime. The important design differences from an earlier design, Reactor B [4], are that: (1) the cavity radii and quartz dome wall radius and height are increased, and (2) Reactor C employs a "non-classical" electromagnetic (EM) TM_0/TEM_{011} plasma excitation applicator mode that allows control of plasma position, size, shape and intensity. Reactor C produces high power density discharges, i.e. 400–1000 W/cm^3, reduces wall heating and wall deposition and provides robust diamond synthesis up to 300 torr. In the Reactor C design the reactor radius varies versus the reactor axial position. This idea has also been employed by other reactor designs [17,18]. SCD synthesis was performed within the 180–300 torr regime, and a diamond growth window was observed between 950 and 1300 °C with SCD growth rates in excess of 75 μm/h. A direct experimental comparison with the earlier Reactor B design [4] indicates that growth rates for Reactor C within the growth window were 1.2–2.5 greater than the corresponding growth rates for Reactor B. Micro-Raman spectroscopy, SIMS and IR–UV transmission spectroscopy measurements showed that the SCD synthesized with Reactor C was of similar quality to type IIa diamond.

References

[1] C.S. Yan, Y.K. Vohra, H.K. Mao, R.J. Hemley, Proc. Natl. Acad. Sci. 99 (2002) 12523.
[2] F. Silva, K. Hassouni, X. Bonnin, A. Gicquel, J. Phys. Condens. Matter 21 (2009) 364202.
[3] Y. Mokuno, A. Chayahara, Y. Soda, Y. Horino, N. Fujimori, Diamond Relat. Mater. 14 (2005) 1743.
[4] K.W. Hemawan, T.A. Grotjohn, D.K. Reinhard, J. Asmussen, Diamond Relat. Mater. 19 (2010) 1446.
[5] K.P. Kuo, J. Asmussen, Diamond Relat. Mater. 6 (1997) 1097.
[6] J. Asmussen, R. Mallavarpu, J.R. Hamann, H.C. Park, Proc. IEEE 62 (1974) 109.
[7] R. Mallavarpu, M.C. Hawley, J. Asmussen, IEEE Trans. Plasma Sci. PS-6 (1978) 341.
[8] P.L. Kapitza, Sov. Phys., JETP 30 (1970) 973.
[9] S. Whitehair, J. Asmussen, J. Propul. Power 3 (1987) 136.
[10] J.E. Brandenburg, J. Kline, D. Sulliven, IEEE Trans. Plasma Sci. 33 (2005) 776.
[11] K.D. Diament, B.L. Ziegler, R.B. Cohen, J. Propul. Power 23 (2007) 27.
[12] S. Offermans, J. Appl. Phys. 67 (1990) 115.
[13] T.A. Grotjohn, J. Asmussen, J. Sivagnaname, D. Story, A.L. Vikharev, A. Gorbachev, A. Kolysko, Diamond Relat. Mater. 9 (2000) 322.
[14] S.S. Zuo, M.K. Yaran, T.A. Grotjohn, D.K. Reinhard, J. Asmussen, Diamond Relat. Mater. 17 (2008) 300.
[15] A. Tallaire, J. Achard, F. Silva, R.S. Sussman, A. Gicquel, Diamond Relat. Mater. 14 (2005) 249.
[16] R. Berman, Physical Properties of Diamond, Oxford University Press, 1965, p. 300.
[17] H. S. Sohn, W. H. Choe, US Patent # 7171919, (2007).
[18] M. Funer, C. Wild, P. Koidl, Appl. Phys. Lett. 72 (1998) 1149.